

Comparison of Iodine-123-Disintegrins for Imaging Thrombi and Emboli in a Canine Model

Linda C. Knight, Alan H. Maurer and Jan E. Romano

Nuclear Medicine Division, Department of Diagnostic Imaging, Temple University School of Medicine, Philadelphia, Pennsylvania

Disintegrins are peptides found in viper venoms which bind to platelets through the glycoprotein IIb-IIIa receptor. The purpose of this work was to evaluate the ability of disintegrins to image thrombi and emboli in vivo. **Methods:** Eight disintegrins (bitistatin, albolabrin, echistatin, eristostatin, kistrin, mambin, halysin and barbourin) were purified from snake venom. After radiolabeling with ^{123}I , disintegrins were tested for their ability to image 24-hr-old experimental deep vein thrombi (DVT) and pulmonary emboli in a canine model. Labeled fibrinogen and platelets were used as controls. Gamma camera imaging was performed during the first 4 hr, after which tissue samples were collected for counting. **Results:** Of the disintegrins tested, ^{123}I -bitistatin had higher uptake in DVT ($0.21 \pm .06\%$ ID/g) than any other disintegrin ($0.009\text{--}0.036\%$ /g, $p < 0.05$). Bitistatin had higher DVT-to-blood ratios (9.8 ± 2.5) than all other disintegrins, ^{125}I -fibrinogen or $^{99\text{m}}\text{Tc}$ -HMPAO-platelets ($p < 0.05$). Images of DVT obtained with ^{123}I -bitistatin were focally positive within 1 hr and improved by 4 hr. In pulmonary emboli, the absolute uptake of ^{123}I -bitistatin ($0.64 \pm 0.17\%$ ID/g) was higher than all other compounds ($p < 0.05$), although barbourin had moderate uptake ($0.23 \pm 0.11\%$ ID/g) and may also be useful for imaging pulmonary embolism (PE). The uptake of bitistatin in PE was superior to both ^{125}I -fibrinogen ($0.18 \pm 0.02\%$ ID/g) ($p < 0.05$) and $^{99\text{m}}\text{Tc}$ -HMPAO-platelets ($0.14 \pm 0.02\%$ ID/g, $p < 0.05$). Iodine-123-bitistatin had embolus-to-blood ratios averaging 27 ± 7 , which was higher than platelets, fibrinogen, echistatin, mambin or halysin ($p < 0.05$). Iodine-123-bitistatin background in lungs, liver and heart were low, which permitted visualization of all pulmonary emboli by 2–4 hr after injection. **Conclusion:** Labeled bitistatin should be investigated further as an agent which may permit rapid imaging of both thrombi and emboli.

Key Words: thrombosis; pulmonary embolism; iodine-123-labeled peptides; platelets

J Nucl Med 1996; 37:476–482

Radiopharmaceuticals which have previously been tested for imaging of deep vein thrombosis (DVT) and pulmonary embolism (PE) suffer from various limitations. For example, radio-labeled platelets and fibrinogen exhibit slow blood clearance and poor binding to mature thrombi, which precludes their ability to rapidly image pre-existing thrombi (1,2). In addition, the separation and labeling procedure for ^{111}In - or $^{99\text{m}}\text{Tc}$ -labeled autologous platelets is tedious, time-consuming and requires handling of the patient's blood. Murine antifibrin antibodies may bind to mature thrombi, but even Fab' fragments have blood clearance rates which are too slow for reliable thrombus imaging within 6 hr after injection (3). With murine antibodies, there is also concern about formation of human anti-mouse antibodies (HAMA) (4) which may preclude repeat examination. In addition to their shortcomings for imaging

peripheral thrombi, most of the previously studied labeled proteins and cells exhibit significant liver uptake, which makes visualization of PE difficult in inferior portions of the lung.

Short synthetic peptides containing a binding site for activated platelets have been investigated for imaging thrombi because they have the advantages of rapid blood clearance and low liver uptake. Unfortunately, the peptides tested to date have exhibited poor binding to pre-existing thrombi (5,6).

In light of these problems, our goal has been to find an agent which will bind in high concentration to pre-existing deposits of platelets or fibrin and which will permit imaging of thrombotic lesions within a few hours after injection. It is hoped that such a tracer would enable direct visualization of pulmonary emboli in addition to peripheral thrombi.

Disintegrins are peptides found in viper venom which bind with high affinity to the surface of activated platelets at the Glycoprotein IIb-IIIa (GP IIb-IIIa) complex. The purpose of the project was to evaluate a variety of radiolabeled disintegrins to determine their potential utility for imaging thrombi and emboli.

MATERIALS AND METHODS

Source of Disintegrins

Eight disintegrins were evaluated in this study. Table 1 lists the amino acid sequences for the compounds tested. Initially, small quantities of bitistatin, albolabrin, echistatin and eristostatin (7) were provided by Drs. McLane and Niewiarowski from the Thrombosis Research Center at Temple University. Subsequently, several additional disintegrins were isolated from crude venom in Dr. Knight's laboratory: bitistatin (from *Bitis arietans* venom) (8), kistrin (from *Calloselasma rhodostoma*) (9), mambin (from *Dendroaspis jamesoni*) (10), halysin (from *Agkistrodon halys*) (11) and barbourin (from *Sistrurus milaris barbouri*) (12).

A general method was developed to separate each active disintegrin from other venom components. First, one gram of crude freeze-dried venom (Miami Serpentarium Laboratories, Punta Gorda, FL) was dissolved in 10–15 ml of 0.05 M ammonium acetate, pH 5.0, and then clarified by ultracentrifugation at 20,000 rpm for 30 min. The supernatant was applied to a $2.6 \times 25\text{-cm}$ column of CM-Sepharose Fast Flow (Pharmacia, Uppsala, Sweden) and eluted with a stepwise gradient of ammonium acetate solutions of increasing pH and ionic strength (from 0.05 M, pH 5.0, to 1.0 M, pH 9.6). The column was run at a flow rate of 15 ml/min and fractions of 3 ml each were collected. Peaks were located by measuring absorbance at 280 nm of every fifth fraction. Peaks containing active disintegrins were identified by their ability to inhibit human platelet aggregation (see below) and then freeze-dried in shallow dishes and stored at -70°C prior to further purification.

The second step in purification utilized reverse-phase HPLC. The freeze-dried material was dissolved in 8% acetonitrile containing 0.1% TFA. The solution was loaded into a $21.4 \times 250\text{-mm}$ C18

Received Jan. 10, 1995; revision accepted May 15, 1995.

For correspondence or reprints contact: Linda C. Knight, PhD, Nuclear Medicine Division, Temple University School of Medicine and Hospital, 3401 N. Broad St., Philadelphia, PA 19140.

TABLE 1
Sequences of Disintegrins*

	10	20	30	40	50	60	70	80
Bitistatin	•							•
	SPFVCGNEIL	EQGEDCDGS	PANCDQCCN	AATCKLTPGS	QCNHGECDDQ	CKFKKARTVC	RIARGDWDD	YCTGKSSDCP
Albolabrin		EAGEDCDGS	PAN---PCCD	AATCKLLPGA	QCGEGLCCDQ	CSFMKKGTTIC	RRARGDLDLD	YCNGISAGCP
Eristostatin				-----QEE	PCATGFCRR	CKFKRAGKVC	RVARGDWDD	YCTGKSCDCP
Echistatin					ECESGPCRR	CKFLKEGTTIC	KRARGDMDDD	YCNGKTCDCP
Kistrin		--GKECDCSS	PEN---PCCD	AATCKLRPGA	QCGEGLCCDQ	CKFSRAGKIC	RIPRGDMFPD	RCTGQSADCP
Barbourin		EAGEEDCSS	PEN---PCCD	AATCKLRPGA	QCADGLCCDQ	CRFMKKGTTVC	RVARGDWDD	RCTGQSADCP
Halysin		EAGEEDCGS	PGN---PCCD	AATCKLRQGA	QCAEGLCCDQ	CRFMKKGTTVC	RIARGDMDDD	YCNGISAGCP
Mambin			---RICYNHL	GTKPPTTEC	TQEDSCYKNI	TFDNIRRGCC	FTPRGDMFPGP	YCCESDKCNL

*After Gould et al. (20).

A = Ala; C = Cys; D = Asp; E = Glu; F = Phe; G = Gly; H = His; I = Ile; K = Lys; L = Leu; M = Met; N = Asn; P = Pro; Q = Gln; R = Arg; S = Ser; T = Thr; V = Val; W = Trp; Y = Tyr.

Note: RGD or KGD sequence is found in residues 64-66.

column, 300Å pore size, 12 µm particle diameter, with a guard column (Rainin column and HPLC system, Woburn, MA). The compounds were eluted with a linear gradient of 8% to 60% acetonitrile in 0.1% TFA, over 60 min, at a flow rate of 16 ml/min. The elution was monitored continuously at 254 nm, and peaks were collected manually as they eluted. Aliquots (10 µl) of peaks were freeze-dried and then tested for aggregation inhibitory activity after redissolution in water. Peaks containing inhibitory activity were pooled and freeze-dried. As necessary, samples were re-chromatographed on reversed-phase HPLC at a shallower gradient until a single peak was present. After purification and freeze-drying, the compounds were dissolved in sterile water for injection and stored as frozen solution at -70°C. Purified disintegrins were analyzed to determine molecular weight and the N-terminal amino acid sequence to verify the purity and identity of the compounds.

In Vitro Testing of Disintegrins

The potency of each compound for inhibiting platelet aggregation was determined by aggregometry (13). Briefly, platelet-rich plasma was prepared from whole blood anticoagulated with 0.1 volume of 3.8% sodium citrate by centrifugation at 180 g for 12 min. Aggregometry studies were done by adding graded doses of each disintegrin or Arg-Gly-Asp-Ser (Sigma, St. Louis) to platelet-rich plasma, waiting 1 min, then adding an aggregatory stimulus (10 µM ADP) (Sigma, St. Louis) and monitoring changes in light transmission in an aggregometer. The control sample contained no disintegrin and its aggregation response was considered to be 100%. The decrease in aggregation from the control was plotted versus disintegrin concentration. From this graph, the concentration of disintegrin required to inhibit aggregation by 50% (IC₅₀) was estimated.

Radiolabeling

Each disintegrin was labeled with ¹²³I for imaging studies as follows: A sample of disintegrin (70 ± 31 µg, mean ± s.d.) was mixed with 100 µl 0.18 M Tris buffer, pH 7.8, and 360 ± 90 MBq (10 ± 3 mCi) ¹²³I. The mixture was then transferred to a septum-capped microfuge tube coated on the inside walls with 100 µg Iodogen™(1,3,4,6-tetrachloro-3α,6α-diphenylglycoluril, Pierce Chemical Co., Rockford, IL). After 30 min at room temperature, the reaction mixture was diluted with 0.5 ml sterile water and drawn up into a syringe. No reducing agent was used. The mixture was allowed to stand in the syringe for 5 min. Free iodide was then removed by combining the reaction solution with AG 1 × 8 ion-exchange resin (Bio-Rad Labs, Hercules, CA) (50% by volume in 0.05 M TRIS, pH 7.4, containing 1% serum albumin). This mixture was passed through a filter with 0.2-µm pores to remove resin and free iodide (14).

Iodine-125-fibrinogen and ^{99m}Tc-HMPAO-labeled autologous platelets were used as controls. Human fibrinogen was radiolabeled with ¹²⁵I by the Iodine Monochloride method (15). Autologous canine platelets were isolated from citrated whole blood by differential centrifugation and were labeled with ^{99m}Tc-HMPAO (Amersham, Arlington Heights, IL) by the method of Becker et al. (16).

In Vivo Testing

Iodine-123-labeled disintegrins were tested for their ability to image thrombi in animal models of PE and DVT. All animal studies were approved by the Institutional Animal Care and Use Committee. Thirty-one male mongrel dogs, averaging 16.8 ± 0.4 kg, were used for the study. After an overnight fast, dogs were anesthetized either with intravenous pentobarbital or with halothane in O₂. The DVT model was created by transcatheter placement of an 8-mm embolization coil in a femoral vein as previously described (17,18). A canine model of PE was created by

releasing 5-mm embolization coils in the inferior vena cava so that the coils embolized to the lungs. Radiographs (without contrast) were taken to document the locations of the coils. The coils were placed 1 day before administration of radiotracers to allow the lesions to mature to approximate the composition of clinical lesions.

On the day of imaging, the dogs were positioned under a gamma camera equipped with LEAP collimator and a 20% window centered on the 159 keV photopeak of ^{123}I . Iodine-123-labeled disintegrin ($70 \pm 3 \mu\text{g}$ labeled with an average of $181 \pm 44 \text{ MBq}$ [$4.9 \pm 1.2 \text{ mCi}$] of ^{123}I) was injected into a foreleg vein followed by a saline flush. Anterior images of the legs (500K counts) and lateral images of the lungs (100K cts) were collected over the next 4 hr in a 200×200 byte matrix using a NuLear Mac computer (Scientific Imaging, Denver, CO). When necessary, lead shielding was placed over the urinary bladder (in the leg views) or over the thyroid (in the lateral chest views). Additional static views of the anterior chest and abdomen were also acquired at hourly intervals and were used for qualitative assessment of the general organ distribution of the radiotracers.

In other studies, 225 MBq (6 mCi) $^{99\text{m}}\text{Tc}$ -HMPAO-labeled autologous platelets were administered in place of ^{123}I -labeled disintegrin. The camera was set to acquire the 140 keV emission of $^{99\text{m}}\text{Tc}$ with a 20% window. All other aspects of the study remained the same. In some studies, 1.3–2.2 MBq (35–60 μCi) ^{125}I fibrinogen ($\sim 0.5 \text{ mg}$) were injected in the same vein and flushed in with saline prior to injecting the imaging radiotracer.

Qualitative Evaluation of Image Appearance

Uptake in the area of lesions was visually graded for intensity of uptake over background: +1 (mild), +2 (moderate), +3 (marked).

Quantitative Tissue Distribution

At the conclusion of the imaging study, the animal was euthanized and samples of tissues and fluids were taken for in vitro analysis. Immediately before euthanasia, a cardiac blood sample was drawn into a heparinized syringe, then dispensed into weighed tubes. The femoral vein containing the coil was dissected free from the point of insertion of the catheter (in the groin crease) distally to beyond the farthest extent of thrombus. The vessel and its contents were removed intact from the body. The vessel was cut open along its length, and the thrombus (including coil) was separated from vessel wall. Thrombus was further separated from coil and dacron fibers and placed on preweighed papers for counting.

The embolized coils were located in excised lungs initially based on location in the chest radiographs and then by direct palpation. Prior to dissection, the excised lungs were drained of blood and placed directly on the collimator face for acquisition of a final image. As with the venous thrombus, the lung coils with associated lesion were kept intact in their vessel segment until the vessel was removed from surrounding tissue, after which embolus, coil, fibers and vessel wall were separated for counting. Each of these samples, as well as samples of skeletal muscle, normal lung and control vessel (femoral vein from the contralateral leg) were weighed before they had a chance to dry. The samples were counted in a NaI(Tl) well counter along with a saved aliquot of the administered dose. Because of downscatter from ^{123}I into the ^{125}I window of the well counter, the samples were re-counted the following week (after decay of ^{123}I) to determine ^{125}I content.

From the above data, the following quantities were determined: the percentage of the injected dose associated with each type of tissue and the ratios of lesion uptake (%ID/g) to uptake in blood, muscle, and lungs. For each quantity, analysis of variance was used to test whether there was a difference between radiopharmaceuticals, with $p < 0.05$ as the criterion for significance. Statistical analyses were performed using StatView II software (Abacus,

TABLE 2
Potency for Inhibition of Platelet Aggregation (nM)

Compound	IC ₅₀ (human)	Ref.	IC ₅₀ (human)	Ref.	IC ₅₀ (canine)
Halysin	262		280	11	220
Albolabrin	185	7	220–309	22,34	n.d.
Bitistatin	165		108–237	7,8,19	168
Echistatin	136	7	101	26	127
Kistrin	90		113–128	10,19	212
Eristostatatin	59	7	59		n.d.
Barbourin	49		113	10	564
Mambin	48		172	10	231
Arg-Gly-Asp-Ser	145,000		205,000	19	197,000

Berkeley CA) in a Macintosh Quadra 800 computer (Apple Computer, Cupertino, CA).

RESULTS

Radiolabeling

The mean labeling efficiency for disintegrins was $48\% \pm 3\%$ (mean \pm s.e.m.). This resulted in an average specific activity after purification of $652 \pm 75 \text{ mCi}/\mu\text{mole}$.

In Vitro Testing

IC₅₀s for inhibition of platelet aggregation are listed in Table 2. All disintegrins were more than 700-fold more potent than the tetrapeptide Arg-Gly-Asp-Ser.

Qualitative Evaluation of Image Appearance

Figure 1 shows the typical locations of coils placed for experimental DVT and PE.

Figure 2 shows examples of DVT images with various radiolabeled disintegrins. Uptake of bitistatin was observed in all DVT (all +3 or +2 intensity). Focal uptake was evident within the first hour after injection, and steadily improved throughout the study. Technetium-99m-platelet uptake permitted visualization of 3/4 lesions with variable focality (+1, +2, +3) because of persistent blood-pool background. The fraction of DVT visualized with other tracers and the focality of visualized lesions were: barbourin 2/3 (+2), kistrin 2/4 (+2), mambin 2/3 (+1), halysin 2/2 (+1, +2), eristostatatin 1/3 (+2), echistatin 1/3 (+2) and albolabrin 0/3. In the negative studies, there was frequently diffuse increased uptake along the entire length of the instrumented femoral vein compared with the control side, but this was interpreted as negative because only focally localized lesions were considered positive for thrombus uptake. Iodine-123-bitistatin displayed less soft-tissue background than the other disintegrins.

Figure 3 shows examples of lung images after injection of ^{123}I tracers. Because of the deep, narrow chest in dogs, emboli

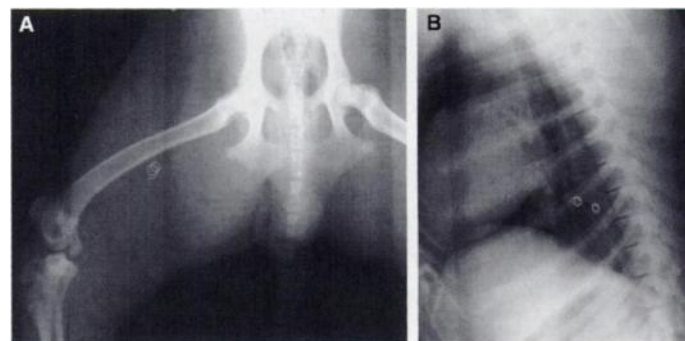


FIGURE 1. Radiographs show typical locations of the coils placed to induce experimental thrombotic lesions. (A) Anterior-posterior view of the right hind leg of a dog with an embolization coil placed in the femoral vein. (B) Lateral view of the chest shows coils in the left lower lobe of the lung.

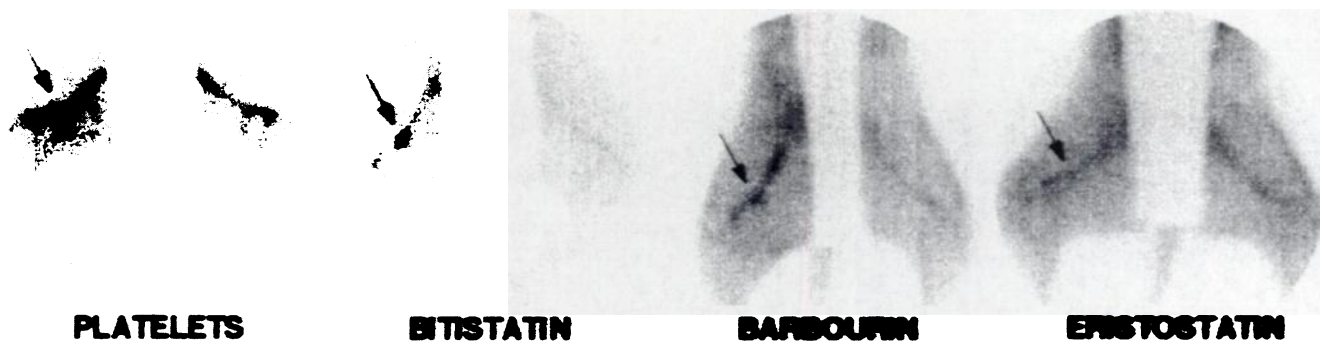


FIGURE 2. Anterior images of the hind legs of dogs 2–4 hr postinjection of ^{123}I -disintegrins or $^{99\text{m}}\text{Tc}$ -HMPAO-labeled autologous platelets. Embolization coils were placed 24 hr before injection of radiotracers, and their locations are indicated by arrows. Lead shielding was placed over the urinary bladder. In each image, 500K counts were acquired; Left to Right: $^{99\text{m}}\text{Tc}$ -HMPAO-labeled platelets localized at the site of thrombus at 4 hr, but persistent blood pool was apparent. Iodine-123-bitistatin demonstrated intense focal uptake by 2 hr, with low background activity. Iodine-123-barbourin displayed moderate uptake at 4 hr, with notable activity along the instrumented femoral vein. Uptake at the site of catheter insertion is visible proximal to the coil location. Iodine-123-eristostatin showed minimal uptake at 4 hr at the site of a small thrombus, with pronounced soft-tissue activity and moderate residual vascular activity.

were best imaged in lateral views. All sites of pulmonary emboli (some sites had two coils) were visualized in all animals studied with bitistatin (all +2 or +3). Pulmonary emboli were also visualized with: barbourin 5/5 (+1 to +3), kistrin 5/5 (+1 to +3), mambin 1/4 (+1), halysin 1/2 (+2; the other not visualized because of an artifact), eristostatin 2/3 (+1) and albolabrin 1/3 (+1). Platelets enabled visualization of only 1/2 emboli (+1). In excised lungs imaged directly on the collimator face, all emboli were visualized with bitistatin, albolabrin, barbourin, kistrin, halysin, platelets and eristostatin and 3/4 were visualized ex vivo with mambin. No emboli were visualized with echistatin, either in vivo or ex vivo.

Based on anterior images of the chest and abdomen, the qualitative organ distribution varied among the disintegrins. Bitistatin concentrated in the spleen but not the liver, thus

providing a clear field for locating pulmonary emboli. In contrast, albolabrin had quite pronounced liver uptake which persisted. Eristostatin, barbourin, kistrin, mambin and halysin had moderate uptake in both liver and kidneys, which cleared substantially by 2 hr. Echistatin was promptly excreted by the kidneys and never displayed significant liver uptake. All disintegrins except bitistatin displayed significant soft-tissue background. Because of the use of an ^{123}I label, which is susceptible to dehalogenation in vivo, stomach and thyroid activity were frequently seen on images acquired more than 1 hr postinjection of disintegrins.

Quantitative Tissue Distribution

The values for uptake of tracers by DVT are shown in Table 3. Bitistatin had the highest absolute uptake (%ID/g lesion) of

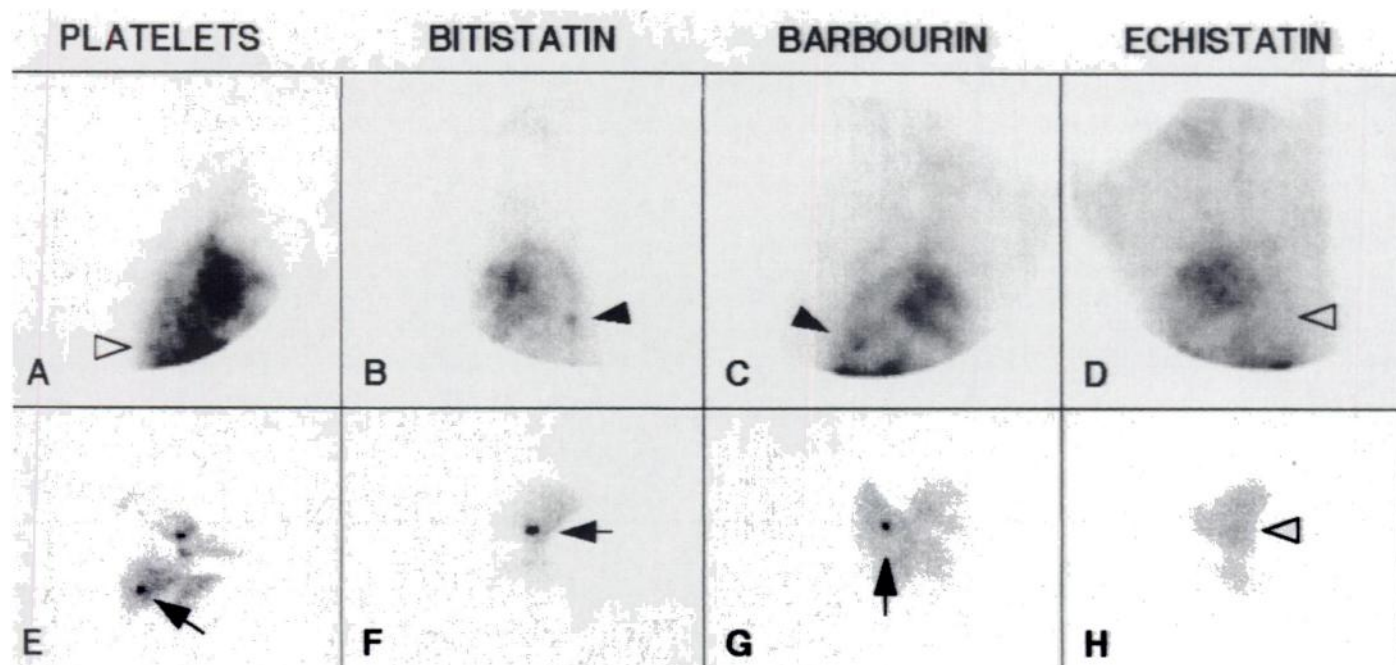


FIGURE 3. (A–D) Planar images of the chests of dogs 3.5 hr postinjection of $^{99\text{m}}\text{Tc}$ -HMPAO-labeled autologous platelets or ^{123}I -disintegrins. Pulmonary emboli had been induced 24 hr previously using embolization coils. Lead shielding was placed over the thyroid. Images were acquired for 1000K counts each. Solid arrows show the locations (confirmed by radiographs) of visualized pulmonary emboli, while outlined arrows show the locations of emboli which were not visualized by scintigraphy. (E–H) Ex vivo images of the lungs from the same animals. The excised lungs were placed directly on the collimator face and counts were acquired for 20 min. Solid arrows indicate the locations of the coils, and the outlined arrow shows the location of a coil not visualized. Left to Right: $^{99\text{m}}\text{Tc}$ -HMPAO-labeled platelets. The embolus was not well visualized in the right lateral view (A), although it was clearly seen in the ex vivo lung image (E); ^{123}I -bitistatin. The embolus was visualized in the left lateral view (B) and also clearly seen in the ex vivo lung image (F); ^{123}I -barbourin. The embolus was visualized in the right lateral view (C) and also clearly seen in the ex vivo lung image (G); ^{123}I -echistatin. The embolus was not visible in either the left lateral view (D) or the ex vivo lung image (H).

TABLE 3
Uptake of Various Compounds in Venous Lesions Four Hours Postinjection

Compound	No.	%ID/g	DVT-to-Blood	DVT-to-Muscle
Bitistatin	6	0.21 ± 0.06	9.8 ± 2.5	125 ± 41
Albolabrin	3	*0.036 ± 0.018	*4.5 ± 2.7	*19 ± 12
Echistatin	3	*0.009 ± 0.001	*1.0 ± 0.2	*3.3 ± 0.7
Eristostatin	3	*0.030 ± 0.014	*2.0 ± 1.1	*9.6 ± 5.6
Kistrin	4	*0.018 ± 0.005	*2.5 ± 0.6	*9.2 ± 2.8
Mambin	3	*0.028 ± 0.003	*4.5 ± 0.8	*16 ± 1
Barbourin	3	*0.028 ± 0.008	*4.2 ± 1.5	*26 ± 18
Halysin	2	*0.029 ± 0.005	*3.9 ± 0.5	25 ± 9
Fibrinogen	27	0.18 ± 0.02	*2.8 ± 0.4	83 ± 11
Platelets	4	0.15 ± 0.06	*5.0 ± 2.3	*230 ± 73

*p < 0.05 vs. bitistatin.

all the disintegrins tested. Bitistatin had significantly higher thrombus-to-blood ratios at 4 hr than any other disintegrin, ¹²⁵I-fibrinogen or ^{99m}Tc-HMPAO-platelets. Thrombus-to-muscle ratios for bitistatin were higher than most other compounds, but were lower than thrombus-to-muscle ratios for platelets.

The values for uptake of tracers by PE are shown in Table 4. Bitistatin had the highest absolute uptake (%ID/g lesion) of all the disintegrins, ¹²⁵I-fibrinogen or ^{99m}Tc-HMPAO-platelets. PE-to-background ratios were also higher for bitistatin compared with most of the other tracers tested. Several compounds, however, had moderate %ID/g as well as PE-to-muscle and PE-to-lung ratios, notably barbourin.

DISCUSSION

Recently, a family of GP IIb/IIIa ligands called disintegrins has been found in viper venoms (19,20). Disintegrins range from about 5 kDa to 9 kDa. All contain the Arg-Gly-Asp (RGD) or Lys-Gly-Asp (KGD) tripeptide sequence common to ligands for the GP IIb/IIIa receptor and they contain multiple disulfide linkages in highly conserved positions. In all of the disintegrins for which the three-dimensional structures have been determined, the RGD sequence is presented to the receptor at the end of a loop structure (21-24). In vitro studies have shown that disintegrins are potent inhibitors of fibrinogen binding to its receptor on platelets (20). In vivo studies with disintegrins have shown that they have potential utility for prevention of platelet aggregation after angioplasty or thrombolytic therapy and they appear to be nontoxic and safer than monoclonal antibodies directed against the same site (9,25,26).

Because of their affinity for activated platelets, disintegrins offered the potential for imaging platelet deposits in vivo. The aim of this study was to evaluate several radiolabeled disintegrins for their ability to bind to thrombi and emboli in vivo and permit rapid imaging. Of the eight disintegrins tested, bitistatin was consistently better than the rest for imaging venous and pulmonary emboli. Several other disintegrins, for example barbourin, appear to have potential for imaging PE.

Mambin is not technically a disintegrin. Although it contains RGD at the apex of a loop structure, the remainder of the molecule has more structural homology with neurotoxic components of snake venom than with the disintegrins (10). It was included in this study to determine the importance of the RGD loop. Although it has high potency in vitro, mambin did not perform as well in vivo as several other disintegrins for imaging thrombotic lesions. It is possible that other aspects of the conformation of certain disintegrins are important for their binding to platelet deposits in vivo.

Despite similarities in amino acid sequences, the disintegrins tested in this project displayed a range of behaviors in vivo with respect to thrombus binding and distribution in normal tissues. The observed differences in thrombus and embolus targeting cannot be explained solely by potency for inhibiting platelet aggregation in vitro. Although ability to bind to activated platelets is certainly a prerequisite for imaging platelet deposits in vivo, neither canine nor human IC₅₀ results would have predicted that bitistatin would be significantly better than the rest.

It is possible that minor differences in structure are responsible for differences in behavior among the disintegrins. The position of the labeling site tyrosine (Y) relative to the RGD is apparently not the determining factor. Kistrin and barbourin (in which the Y is outside the R(K)GD loop) were not superior to bitistatin (in which the Y is inside the RGD loop, as in echistatin, eristostatin, albolabrin, and halysin). The hydrophobicity of the residue adjacent to RGD (X in RGD_X) has been shown to be important in barbourin and other disintegrins for determining specificity for the GPIIb/IIIa receptor in vitro (27). Among the disintegrins tested in this project, X can be W (Trp), M (Met) or D (Asp). We used the hydrophobic nature as a criterion and found the expected order of potency would be bitistatin, barbourin and eristostatin (RGDW) > kistrin, mambin (RGDM) > albolabrin, halysin, echistatin (RGDD). We found that the %ID/g in PE appeared to follow a similar order: bitistatin > barbourin, eristostatin > albolabrin, kistrin, mambin, halysin, echistatin (no significant difference among the last five). This indicates that the order of avidity may be

TABLE 4
Uptake of Various Compounds in Pulmonary Emboli Four Hours Postinjection

Compound	No.	%ID/g	PE-to-Blood	PE-to-Muscle	PE-to-Lung
Bitistatin	11	0.64 ± 0.17	27 ± 7	360 ± 109	46 ± 16
Albolabrin	4	*0.12 ± 0.05	14 ± 5	*65 ± 31	*12 ± 4
Echistatin	4	*0.009 ± 0.001	*1.0 ± 0.03	*3.3 ± 0.3	*2.5 ± 1.8
Eristostatin	5	*0.21 ± 0.06	12 ± 4	*56 ± 18	*15 ± 5
Kistrin	8	*0.11 ± 0.05	20 ± 11	*53 ± 23	*10 ± 6
Mambin	5	*0.070 ± 0.022	*12 ± 4	*38 ± 10	*11 ± 6
Barbourin	6	*0.23 ± 0.11	16 ± 8	*105 ± 71	26 ± 12
Halysin	4	*0.034 ± 0.003	*4.5 ± 0.5	*28 ± 5	*5.1 ± 0.5
Fibrinogen	35	*0.18 ± 0.02	*2.7 ± 0.3	*88 ± 16	*11 ± 3
Platelets	2	*0.14 ± 0.02	*4.1 ± 0.7	249 ± 62	9

*p < 0.05 vs. bitistatin.

†p < 0.05 vs. barbourin.

related in part to the nature of X in RGD_X, with W more favorable than M or D. It is not known, however, what structural features account for the marked difference in binding between bitistatin and the other disintegrins which contain RGDW. This question remains to be answered in future studies.

Labeled fibrinogen and platelets were used for comparison in these studies so that the labeled disintegrins could be compared to standards which have been well-characterized. Radiolabeled fibrinogen has been used for clinical imaging of acute DVT (28) because it has excellent uptake into actively forming thrombi (1). One major limitation has been its long residence in the blood pool, which hampered the ability to image a lesion over the blood background for up to 24 hr. Radiolabeled platelets have provided useful images of platelet deposition in both venous and arterial lesions and occasionally have demonstrated pulmonary emboli (2,29). Imaging delays of up to 3 days, however, may be needed for adequate reduction in blood background, especially in the chest. In this study, Figure 3 shows that labeled platelets bound to the emboli created in our model, as they were visualized *ex vivo*. The lesions, however, were not reliably visualized *in vivo* because of excessive blood activity. The results obtained with bitistatin suggest that it has lesion uptake equivalent or superior to fibrinogen and platelets but has more rapid disappearance from the blood background which permits imaging of lesions within a few hours.

The uptake of bitistatin may also be compared with other radiotracers which have been previously evaluated by us in the same model of DVT. Bitistatin had higher uptake and higher target-to-background ratios in venous thrombi than did ^{99m}Tc-antifibrin antibody T2G1s Fab' (0.089%ID/g, DVT/blood = 4, DVT/muscle = 69 at 4 hr postinjection) (17). Subsequent clinical trials of labeled antifibrin antibodies indicated that the canine model accurately predicted the focality of uptake and the persistence of blood background activity (3,30). Thus, the studies reported here suggest that labeled bitistatin may be superior to antifibrin antibody fragments for imaging DVT clinically.

In other studies in the same animal model, synthetic linear peptides of 17 amino acids containing the Arg-Gly-Asp sequence were also tested for their ability to image thrombi (6). The small peptides displayed much lower uptake (0.006%/g in DVT) than bitistatin (0.21%/g in DVT). Attempts were made to improve the affinity for the receptor by synthesizing short peptides containing an analog for Arg-Gly-Asp which is constrained into a loop structure. This succeeded in lowering the IC₅₀ for inhibition of platelet aggregation but the cyclic peptides did not display improved lesion uptake in this model (0.007%/g in DVT) (5). The studies reported here have shown that potency for inhibiting platelet aggregation *in vitro* does not necessarily correlate with thrombus uptake *in vivo*.

The disintegrins tested in this project were isolated from natural venoms by sequential ion-exchange and reversed-phase liquid chromatography. This technique could be used to prepare sufficient quantities of suitable material for a clinical trial, although isolation from small batches of natural venom is not practical for large-scale production. To date, most published studies with disintegrins have used material obtained by similar methods of isolation from natural snake venom, but some disintegrins have been successfully produced by solid-phase peptide synthesis (12,31) or by recombinant DNA expression in nonmammalian cells such as yeast (32,33). The products folded correctly and were physically and functionally indistinguishable from the native peptides. It should be possible to produce large quantities of bitistatin or other disintegrins by one of these methods rather than by isolation from natural snake venom.

In this project, we used a ¹²³I label because it was the easiest approach for initial labeling of peptides containing tyrosine. One disadvantage of the radioiodine label is dehalogenation *in vivo*, which leads to background uptake in thyroid and stomach, as well as diffuse soft-tissue activity. Stomach and thyroid activity did not affect our ability to image PE. Soft-tissue background was noticeable with most of the disintegrins other than bitistatin. Because images of thrombi and emboli were clearly positive with labeled bitistatin by 2–4 hr postinjection, a ^{99m}Tc label would be well-suited to this agent. If suitable linkers were used for attachment of reduced technetium, this label could be more stable *in vivo* than a radioiodine label.

CONCLUSION

The results of this study demonstrate that the disintegrin bitistatin has very favorable characteristics for imaging DVT and PE in our animal model and suggest that further studies in humans should be pursued.

ACKNOWLEDGMENTS

We are grateful to Stefan Niewiarowski, MD, PhD, and Mary Ann McLane, PhD, for generously providing the disintegrins and for helpful discussions, and to Jeanne Corman and Ram Seetharam, PhD, for peptide sequencing and molecular weight analysis. We also thank Stephanie Buczala, Rosemarie Vosacek, Kevin Brown and David Weston for excellent technical assistance, Milne Hewish for photography and GE Medical Systems for support. Financial support was provided by the Ben Franklin Partnership and DuPont Merck Pharmaceutical Company.

REFERENCES

1. Coleman RE, Harwig SSL, Harwig JF, Siegel BA, Welch MJ. Fibrinogen uptake by thrombi: effect of thrombus age. *J Nucl Med* 1975;16:370–373.
2. Ezekowitz MD, Pope CF, Sostman HD, et al. Indium-111-platelet scintigraphy for the diagnosis of acute venous thrombosis. *Circulation* 1986;73:668–674.
3. deFaucal P, Peltier P, Planchon B, et al. Evaluation of ¹¹¹In-labeled antifibrin monoclonal antibody for the diagnosis of venous thrombotic disease. *J Nucl Med* 1991;32:785–791.
4. Seccamani E, Riva P, Comandini A, et al. HAMA detection in patients submitted to murine monoclonal antibodies administration [Abstract]. *J Nucl Med* 1989;30(suppl):908.
5. Knight LC, Lister-James J, Dean RT, Maurer AH. Evaluation of ^{99m}Tc-labeled cyclic peptides for thrombus imaging [Abstract]. *J Nucl Med* 1993;34(suppl):17P.
6. Knight LC, Radcliffe R, Maurer AH, Rodwell JD, Alvarez VL. Thrombus imaging with technetium-99m synthetic peptides based upon the binding domain of a monoclonal antibody to activated platelets. *J Nucl Med* 1994;35:282–288.
7. McLane MA, Kowalska MA, Silver L, Shattil SJ, Niewiarowski S. Interaction of disintegrins with the alpha IIb beta 3 receptor on resting and activated human platelets. *Biochem J* 1994;301:429–436.
8. Shebuski RJ, Ramjit DR, Bencen GH, Polokoff MA. Characterization and platelet inhibitory activity of bitistatin; a potent arginine-glycine-aspartic acid-containing peptide from the venom of the viper *Bitis arietans*. *J Biol Chem* 1989;264:21550–21556.
9. Yasuda T, Gold HK, Leinbach RC, et al. Kistrin, a polypeptide platelet GPIIb/IIIa receptor antagonist, enhances and sustains coronary arterial thrombolysis with recombinant tissue-type plasminogen activator in a canine preparation. *Circulation* 1991;83:1038–1047.
10. McDowell RS, Dennis MS, Louie A, Shuster M, Mulkerrin MG, Lazarus RA. Mambin, a potent glycoprotein IIb-IIIa antagonist and platelet aggregation inhibitor structurally related to the short neurotoxins. *Biochemistry* 1992;31:4766–4772.
11. Huang TF, Liu CZ, Ouyang CH, and Teng CM. Halyisin, an antiplatelet Arg-Gly-Asp-containing snake venom peptide as fibrinogen receptor antagonist. *Biochem Pharmacol* 1991;42:1209–1219.
12. Scarborough RM, Rose JW, Hsu MA, et al. Barbourin. A GPIIb-IIIa-specific integrin antagonist from the venom of *Sistrurus m. barbouri*. *J Biol Chem* 1991;266:9359–9362.
13. Born GVR, Cross MJ. The aggregation of blood platelets. *J Physiol* 1963;168:178–195.
14. Haisma HJ, Hilgers J, and Zurawski VRJ. Iodination of monoclonal antibodies for diagnosis and radiotherapy using a convenient one-vial method. *J Nucl Med* 1986;27:1890–1895.
15. McFarlane AS. *In vivo* behavior of ¹³¹I-fibrinogen. *J Clin Invest* 1963;42:346–361.
16. Becker W, Börner W, Borst U. Technetium-99m-hexamethyl-propyleneamineoxime (HMPAO) as a platelet label: evaluation of labeling parameters and first *in vivo* results. *Nucl Med Commun* 1988;9:831–842.

17. Knight LC, Maurer AH, Ammar IA, et al. Technetium-99m-antifibrin Fab' fragments for imaging venous thrombi: evaluation in a canine model. *Radiology* 1989;173:163-169.
18. Knight LC, Abrams MJ, Schwartz DA, et al. Preparation and preliminary evaluation of technetium-99m-labeled Fragment E₁ for thrombus imaging. *J Nucl Med* 1992;33:710-715.
19. Dennis MS, Henzel WJ, Pitti RM, et al. Platelet glycoprotein IIb-IIIa protein antagonists from snake venoms: evidence for a family of platelet-aggregation inhibitors. *Proc Natl Acad Sci USA* 1990;87:2471-2475.
20. Gould RJ, Polokoff MA, Friedman PA, et al. Disintegrins: a family of integrin inhibitory proteins from viper venoms. *Proc Soc Exp Biol Med* 1990;195:168-171.
21. Adler M, Carter P, Lazarus RA, Wagner G. Cysteine pairing in the glycoprotein IIb/IIIa antagonist kistrin using NMR, chemical analysis and structure calculations. *Biochemistry* 1993;32:282-289.
22. Calvete JJ, Schäfer W, Soszka T, et al. Identification of the disulfide bond pattern in albolabrin, an RGD-containing peptide from the venom of *Trimeresurus albolabris*: significance for the expression of platelet aggregation inhibitory activity. *Biochemistry* 1991;30:5225-5229.
23. Cooke RM, Carter BG, Murray-Rust P, Hartshorn MJ, Herzyk P, Hubbard RE. The solution structure of echistatin: evidence for disulphide bond rearrangement in homologous snake toxins. *Protein Engineering* 1992;5:473-477.
24. Saudek V, Atkinson RA, Pellon JT. Three-dimensional structure of echistatin, the smallest active RGD protein. *Biochemistry* 1991;30:7369-7372.
25. Shebuski RJ, Ramjit DR, Bencen GH, Pokoloff MA. Effect of bitistatin, a potent RGD-containing peptide from the venom of *Bitis arietans*, on platelet aggregation and bleeding time in the dog [Abstract]. *Circulation* 1989;80(suppl II):422.
26. Shebuski RJ, Ramjit DR, Sitko GR, Lumma PK, Garsky VM. Prevention of canine coronary artery thrombosis with echistatin, a potent inhibitor of platelet aggregation from the venom of the viper, *Echis carinatus*. *Thromb Haemostas* 1990;64:576-581.
27. Scarborough RM, Rose JW, Naughton MA, et al. Characterization of the integrin specificities of disintegrins isolated from American pit viper venoms. *J Biol Chem* 1993;268:1058-1065.
28. DeNardo S, Bogren H, DeNardo G. Detection of thrombophlebitis in the lower extremities: a regional comparison of ¹²³I-fibrinogen scintigraphy and contrast venography. *Am J Roentgenol* 1985;145:1045-1052.
29. Clarke-Pearson DL, Coleman RE, Siegel R, Synan IS, Petry N. Indium-111-platelet imaging for the detection of deep venous thrombosis and pulmonary embolism in patients without symptoms after surgery. *Surgery* 1985;98:98-104.
30. Alavi A, Palevsky HI, Gupta N, et al. Radiolabeled antifibrin antibody in the detection of venous thrombosis: preliminary results. *Radiology* 1990;175:79-85.
31. Garsky VM, Lumma PK, Freidinger RM, et al. Chemical synthesis of echistatin, a potent inhibitor of platelet aggregation from *Echis carinatus*: synthesis and biological activity of selected analogs. *Proc Natl Acad Sci USA* 1989;86:4022-4026.
32. Jacobson MA, Forma FM, Buenaga RF, et al. Expression and secretion of biologically active echistatin in *Saccharomyces cerevisiae*. *Gene* 1989;85:511-516.
33. Hofmann KJ, Schultz LD. Mutations of the alpha-galactosidase signal peptide which greatly enhance secretion of heterologous proteins by yeast. *Gene* 1991;101:105-111.
34. Williams J, Rucinski B, Holt JC, Niewiarowski S. Elegatin and albolabrin purified peptides from viper venoms: homologies with the RGDS domain of fibrinogen and von Willebrand factor. *Biochim Biophys Acta* 1990;1039:81-89.

Angiotensin-Converting Enzyme Inhibition-Induced Changes in Hippurate Renography and Renal Function in Renovascular Hypertension

C. Antoinette Visscher, Dick de Zeeuw, Paul E. de Jong, D. Albertus Piers, Henk Beekhuis, Geny M.M. Groothuis and Roel M. Huisman

Division of Nephrology, Department of Medicine, and Departments of Nuclear Medicine and Pharmacology and Pharmacotherapeutics, Groningen Institute for Drug Studies, University Hospital, Groningen, The Netherlands

We studied the mechanism of angiotensin-converting enzyme (ACE) inhibition-induced changes in hippurate renography of the poststenotic kidney. **Methods:** Ten male mongrel dogs, six with unilateral and four with bilateral renal artery stenosis, were equipped with renal artery blood flow probes and catheters in the aorta, atrium and both renal veins. **Results:** Enalaprilat (10 mg intravenously) in conscious dogs with renal artery stenoses produced changes in all stenotic ($n = 11$) but not in nonstenotic kidney ¹²³I-hippurate renograms ($n = 6$). Renographic changes correlated significantly with initiation of intrarenal ¹³¹I-hippurate retention, a decrease in mean arterial pressure (MAP), renal extraction of ¹³¹I-hippurate and ¹²⁵I-iothalamate ($r = 0.68$, $r = 0.62$, $r = 0.84$, $r = 0.83$, respectively) but not with renal blood flow changes ($r = 0.34$). Furthermore, renal uptake of ¹³¹I-hippurate and ¹²⁵I-iothalamate decreased in stenotic kidneys with a grade II renogram ($-52 \pm 11\%$ and $-79 \pm 6\%$, respectively). Iodine-125-hippurate autoradiograms of stenotic kidneys during ACE inhibition showed tracer retention mainly in the proximal tubular cells. Results during osmotic diuresis supported our findings. **Conclusion:** Angiotensin-converting enzyme inhibition-induced hippurate retention curves of poststenotic kidneys appear to result from a sequence of events. A decrease in MAP combined with efferent vasodilation leads to a decrease in intraglomerular capillary pressure. This decrease in pressure causes a decrease in glomerular filtration rate and proximal tubular urine flow. This decrease in turn hampers tubular hippurate transit and transport across the luminal membrane, leading to intrarenal hippurate

retention and, in more severe cases, decreased renal hippurate uptake.

Key Words: renovascular hypertension; glomerular filtration rate; radioisotope renography; renal artery stenosis; renin-angiotensin system

J Nucl Med 1996; 37:482-488

Renovascular hypertension, the most common form of secondary hypertension, is potentially curable by surgical and radiologic intervention, but a reliable screening test is needed. The best screening test to date appears to be hippurate renography during angiotensin-converting enzyme (ACE) inhibition (1). Technetium-99m-MAG3, a radiopharmaceutical with properties similar to hippurate, has been recently introduced in lieu of hippurate (2). ACE inhibition considerably enhances the sensitivity of hippurate renography for detection of significant renal artery stenosis because ACE inhibition induces a typical pattern of delayed time-to-peak or slowed tracer excretion in the kidney behind a narrowed renal artery (1-4). The mechanism for this altered tracer handling is not completely understood. Several explanations have been advanced, such as a reduced tubular extraction of hippurate (5) or a delay of tracer in the tubular lumen (2,6). A decrease in renal tracer uptake does not explain the change in shape of the renographic curve, which is most likely caused by tubular tracer delay or a combination of tubular tracer delay and reduced renal tracer uptake. To identify the mechanism of ACE inhibition-induced altered hippurate handling, it is necessary to measure simultaneously several

Received Feb. 6, 1995; revision accepted Jul. 14, 1995.

For correspondence or reprints contact: Roel M. Huisman, MD, Division of Nephrology, Department of Medicine, University Hospital, P.O. Box 30.001, 9700 RB Groningen, The Netherlands.